Results in Engineering 28 (2025) 107256

Contents lists available at ScienceDirect

Results in Engineering

journal homepage: www.sciencedirect.com/journal/results-in-engineering

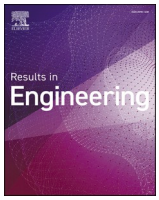

Research paper

Influence of solution treatment on microstructure and mechanical properties of duplex stainless steel prepared by powder metallurgy technique

Ramajayam Mariappan [a], Rasaiah Naveenkumar [b], Thangaraj Vinod Kumar [c], Vadivelu Kannan [d], Prajith Prabhakar [e], Vinayagam Mohanavel [f], Manickam Ravichandran [g,*]

[a] Department of Physics, Saranathan College of Engineering, Venkateshwara Nagar, Tiruchirappalli, Tamil Nadu 620012, India
[b] Department of Mechanical Engineering, SRM Institute of Science and Technology, Vadapalani Campus, Chennai 600026, Tamil Nadu, India
[c] Department of Mechanical Engineering, Vels Institute of Science, Technology and Advanced Studies, Pallavaram, Chennai, Tamil Nadu 600117, India
[d] Department of Physics, K.Ramakrishnan College of Engineering, Samayapuram, Tiruchirappalli 621112, Tamilnadu, India
[e] Department of Mechanical Engineering, Saveetha School of Engineering, Saveetha Institute of Medical and Technical Sciences (SIMATS), Chennai, Tamil Nadu 602105, India
[f] Centre for Sustainable Materials Research, Department of Mechanical Engineering, Academy of Maritime Education and Training (AMET), Deemed to be University, Kanathur, Chennai 603112, Tamil Nadu, India
[g] Department of Mechanical Engineering, K.Ramakrishnan College of Engineering, Samayapuram, Tiruchirappalli 621112, Tamil Nadu, India

ARTICLE INFO

Keywords:
Duplex stainless steel (DSS)
Solution treatment
Powder metallurgy
Sintering atmosphere
Microstructure and Mechanical Properties

ABSTRACT

This study investigates the influence of solution treatment on the microstructure, mechanical properties of powder metallurgy duplex stainless steels (DSS) developed from 316 L and 430 L powders. The sintered DSS samples were annealed at two distinct temperatures of 1150 °C and 1250 °C, followed by water quenching. Comprehensive characterization, including optical microscopy, scanning electron microscopy (SEM), and energy dispersive spectroscopy (EDS), was conducted to evaluate phase distribution and elemental composition. Mechanical properties were assessed through tensile strength, hardness, and elongation tests. The findings reveal that solution treatment enhances densification, particularly at higher annealing temperatures, promoting a homogenous austenite-ferrite phase distribution. For DSS sintered in partial vacuum and solution treated at 1250 °C, densification reached 7.72 g/cm^3 (98.1 % of theoretical density). Significant improvements in tensile strength (up to 824 MPa) and yield strength (up to 438 MPa) were observed. DSS sintered in partial vacuum exhibited superior densification and mechanical performance compared to those sintered in hydrogen. This is due to the minimized oxidation, enhanced diffusion kinetics, and reduced residual porosity achieved in partial vacuum conditions, which collectively improve densification and mechanical stability. These enhanced properties make the treated DSS suitable for applications in marine environments, chemical processing equipment, oil and gas pipelines, and structural components in corrosive or high-stress conditions. The optimized balance between strength and ductility also positions these materials as viable candidates for high-performance automotive and aerospace components.

1. Introduction

Heat treatment has a major sensible and valuable role in making steels, which influences strongly on the phase structures and properties of the steels [1]. Independently, 316 L austenitic stainless steel could serve for remarkable ferritic phase, only at elevated temperature by which the stabilizing elements can execute [2]. In 2009, Hua Tan was reported that an improvement in ferrite volume could be obtained due to γ→α transformation only on high temperature heat treatment of super DSS [3]. Although duplex steels have great qualities, stability is determined by heating conditions. While sustained exposure at 280 °C results in the production of α'-phase, which lowers performance and necessitates stringent thermal management, secondary phases appear between 300 and 1000 °C [4]. High temperatures do not produce a completely

* Corresponding author.
E-mail address: smravichandran@hotmail.com (M. Ravichandran).

https://doi.org/10.1016/j.rineng.2025.107256
Received 28 May 2025; Received in revised form 9 September 2025; Accepted 12 September 2025
Available online 12 September 2025

ferritic structure, but they do improve corrosion resistance and refine microstructure. Heating to 1000–1150 °C and then carefully cooling is necessary for quench hardening. Rapid quenching maintains duplex balance, reduces dislocation density, but may result in coarse element segregation [5].

Research on duplex stainless steels made by laser powder bed fusion (LPBF) and selective laser melting (SLM) shows build orientation, scan strategy, and post-processing affect microstructure and corrosion. Higher angles improve corrosion, moderate angles balance strength, while solution annealing enhances ductility and corrosion resistance [6]. Standard 2205 and super duplex 2507 steels produced by LPBF exhibit ferritic microstructures, with post-treatments solution annealing and hot isostatic pressing (HIP) restoring the duplex structure [7]. 2205 DSS produced via SLM using gas-atomized powder achieved 99.1 % relative density after annealing, which restored a duplex microstructure with ferrite content near 52–56 % depending on measurement method [8]. SLM-fabricated DSS UNS S31803 shows ferritic structure; heat treatments promote austenite, improving elongation, while as-built samples retain higher tensile strength [9]. This study examines how SLM-controlled volumetric energy density (VED) influences SS 310, finding optimal strength and ductility at 56 J/mm^3, where fine grains enhance properties, while higher energy causes coarsening and reduced boundary density [10]. Strong bonding was demonstrated using Super DSS clads on LPBF made low-carbon steel. While heat treatment increased δ–γ balance, decreased strains, and improved corrosion resistance, higher scan speeds decreased austenite [11]. This study examines spin-formed 304 stainless steel bellows under solid solution treatment. Findings reveal transformation of strain-induced martensite into austenite, with grain refinement, reduced microhardness from 379 to 66 HV, conversion of tensile to compressive residual stresses, and significantly improved resistance to stress corrosion, enhancing overall mechanical performance [12]. This study investigates the tensile behaviour of low-nickel duplex stainless steel SUS821L1 across 233–293 K under quasi-static and dynamic loading using a cooled split-Hopkinson tensile bar. Results show increasing flow stress with decreasing temperature, strong temperature sensitivity under quasi-static conditions, and strain-induced martensite reducing stress differences between loading modes [13].

By demonstrating that temperature plays a crucial role in controlling secondary phases, phase stability, and microstructure, researchers emphasize the impacts of heat treatment on duplex stainless steels. This improves mechanical strength and corrosion resistance in both additive and conventional processing [14]. Ageing treatment of DSS at 900 °C promotes rapid chi and sigma phase precipitation, increasing hardness, while heat treatment at 1000 °C dissolves sigma phase, resulting in mechanical properties governed by the balanced ferrite–austenite phase distribution [15]. Studies on stainless steels reveal microstructure and alloying elements govern corrosion resistance. Dislocations, grain boundaries, and molybdenum enhance passive film stability, improving performance in harsh environments like lead-bismuth eutectic and chloride solutions [16]. Molybdenum (Mo) in 2205 DSS enhances passive film stability in 3.5 wt % NaCl by supporting both α- and γ-phase interactions, improving pitting resistance and repassivation, with *Mo species* showing superior protective and recovery capabilities under high potentials [17]. This study evaluates failure mechanisms and erosion resistance of duplex stainless steel (DSS) 2605 N and newly developed DSS 00Cr22Ni6MnMoCu. The novel alloy, with balanced duplex microstructure and optimized alloying elements, exhibited superior resistance to corrosion, abrasion, and erosion, demonstrating 14-fold higher erosion resistance compared to conventional DSS 2605 N [18]. Duplex and super DSS surface modification enhances wear and biological applications [19]. In order to optimize parameters, improve mechanical and wear resistance, maintain corrosion behaviour, and evaluate secondary phase precipitation during heat exposure, this article examines developments in diffusion treatments with a focus on nitriding of duplex and super DSS [20].

According to this article, duplex stainless steel cladding layers, triple-layer cladding offers the best hardness, corrosion resistance, and fretting wear because of its increased Ni and Cr content, lower dilution, and repeated heat cycling [21]. This study analyses the solution annealing of PBF-LB/M-processed X2CrNiMoN25–7–4 DSS and demonstrates that a 3-minute annealing time maximizes strength and corrosion resistance, whereas longer times result in grain coarsening and performance degradation [22]. This research demonstrated 2507 DSS made by LPBF, which combines the benefits of austenitic and ferritic alloys. Results show that it is suitable for high-performance components in demanding engineering applications due to its exceptional strength and resistance to corrosion [23]. In many material preparations techniques, the choice of pre-etchant will affect the degree of microstructural characteristics. Pre-etchant's gradual impact on the materials revealed subtle microstructural characteristics. Furthermore, the hold duration at a particular peak temperature and the peak temperature experienced determine the rate of etching [24]. Using small tensile samples, this study investigates the mechanical characteristics of 120 mm hollow DSS tubes throughout their construction height. The wire feed rate of 1.5 m/min and the travel speed of 60 cm/min produced the best results [25]. For the necessary qualities, choosing the right forming method is essential. ER-80SG filler increases yield strength in MIG-welded E410 steels while decreasing toughness and ductility [26]. Since the regulated temperature input and the advantageous development of acicular ferrite, Widmanstatten, and pearlite in the weld and heat-affected zones, E250 and E410 steels exhibit better mechanical performance with cold metal transfer (CMT) MIG welding than with traditional MIG [27]. This study examines dissimilar welds of SS316L and SS439 produced by Cold Metal Transfer using E309L and E2209 fillers. Due to their duplex microstructure, E2209 weld zones exhibited higher hardness and, in chloride solution, demonstrated superior corrosion resistance with lower current density and more favourable potential than E309L welds [28]. By strengthening Σ3 boundaries, refining precipitates, and delaying $M_{23}C_6$ coarsening, boron addition improves P91 steel's creep resistance and improves high-temperature stability in the heat-affected zone without changing grain size or microhardness [29].

In this present investigation, solution annealing was carried out for sintered DSS developed from 316 L and 430 L powders at two different temperatures such as 1150 °C & 1250 °C and subsequently quenched in water. Microstrctural examinations and mechanical properties evaluation were examined for the solution treated DSS with the impact of sintering atmosphere and solution treatment temperature on austenite and ferrite phase structure.

2. Experimental investigation

This research was mainly focused on effect of two different solution treatment temperatures on microstructure and mechanical properties of powder metallurgy DSS received at sintered condition in two dissimilar conditions. The sintered duplex steel chemical structure was shown in Table 1 has taken in to account the sensitivity of annealing. When Cr increased to the steels, it refines the grain structure. Generally, the strength and toughness can be increased due to grain refinement. Moreover, it has a solubility of 13 % in γ and unlimited solubility in α ferrite. This research works also explained about the solution annealing on the cylindrical duplex steel samples of Φ 30 mm X 12 mm height sintered in different atmospheres, because it controls the re-oxidation by lowering the oxygen content of cooling zone. One set of the samples was sintered in hydrogen gas at a controlled flow rate of 250 ml/min, while the other set was sintered in a partial vacuum at a pressure level of 10^{-1} mbar with backfilling of hydrogen. The average particle sizes of the powders used for the powder metallurgy process were 45 μm for 316 L stainless steel powder and 50 μm for 430 L stainless steel powder.

The solution annealing has been carried out in two different temperatures say 1150 °C and 1250 °C on sintered samples in electrical muffle furnace for one hour and followed by water quenching. The

Table 1
Chemical composition of duplex stainless steels.

Composition	Elemental Concentration (%wt)								
	Cr	C	Ni	Si	Mn	Mo	Fe	Cr_{eq}	Ni_{eq}
DSS A	16.58	0.018	6.22	1.05	0.10	1.10	Bal	19.26	6.81
DSS B	18.93	0.016	8.59	0.95	0.09	3.99	Bal	24.35	9.12

metallographic samples were polished with emery sheets and diamond paste. The sintered sample densities were evaluated using the Archimedes principle, employing distilled water as the immersion medium. The microstructural analysis was done by optical microscopy using an Image Analyzer software aided with berahaa reagent (20 ml HCl+ 80 ml H_2O + 0.3 g Potassium Meta bi-Sulphide) etchant which made coloring on both phases and the Scanning electron microscopy was utilized for obtaining magnified view of both phases and precipitations if any, and the observation on ferrite structure by electrolyte etchant and Energy Dispersive Spectroscopy (EDS) analysis of both solution treated samples were evaluated. A digital tensometer was used to conduct tensile testing at a strain rate of 1 mm/min. Tensile strength was assessed after micro tensile samples were machined in accordance with ASTM E8 standards. A Rockwell Hardness Tester (FIE Model) was used to determine the samples' hardness and a scale with a diamond intender and a 60 kg main load was employed.

Cr_{eq} and Ni_{eq} are obtained through equations from Schaffler's diagram using the Eqs. (1) and (2) [30]

$$Creq = \%\ Cr\ +\ \%\ Mo\ +\ 1.5\ x\ \%\ Si\ +\ 0.5\ x\ \%\ Nb \quad (1)$$

$$Nieq\ =\ \%\ Ni\ +\ 30\ x\ \%\ C\ +\ 0.5\ x\ \%\ Mn \quad (2)$$

3. Results and discussion

3.1. Solution treated properties at 1150 °C of powder metallurgy DSS sintered in two different atmosphere

3.1.1. Densification characteristics

It was observed that solution annealed treatment of 1150 °C, which enhance the dissolution of various elements such as Ni, Cr, Mo and other intermetallics in austenite and ferrite matrix. At higher solution annealing temperatures, the austenite and other intermetallic phases tend to transform into the ferrite phase due to enhanced diffusion and phase stability dynamics [3]. The Diffusion kinetics of ferrite is hundred times faster than the austenitic phase due to the BCC structure. Hence solution treated DSS shows increased density than the sintered one regardless of the sintering environment. The densification characteristics of solution treated DSS at 1150 °C was shown in Table 2.

The densification properties of DSS A and B after solution treatment at 1150 °C in various sintering atmospheres was shown in Table 2. DSS A obtained a sintered density of 7.285 g/cm³ (93.5 % of theoretical density) in the hydrogen-sintered state. Following solution treatment, this density marginally increased to 7.350 g/cm³ (94.5 %). A similar pattern was seen in DSS B, where treatment improved the sintered density from 7.270 g/cm³ (92.3 %) to 7.370 g/cm³ (93.6 %). Both DSS grades showed noticeably greater densification levels when sintered in a partial vacuum. After treatment, DSS A sintered density increased to 7.605 g/cm³ (97.6 %) and then to 7.630 g/cm³ (97.9 %). Additionally, DSS B demonstrated enhanced densification; following solution treatment, values increased from 7.610 g/cm³ (96.6 %) to 7.632 g/cm³ (97.0 %). According to these findings, partial vacuum sintering produces densities that are substantially closer to the theoretical values than hydrogen sintering, demonstrating its superior ability to promote densification. It is anticipated that improved densification will improve the duplex stainless steels' mechanical characteristics.

Table 2
Densification characteristics of solution treated DSS at 1150 °C.

Composition	Sintered Atmosphere	Sintered Density (g/cm³)	Solution Treated Density (g/cm³)	Theoretical Density (g/cm³)
DSS A	Hydrogen	7.285 (93.5 %)	7.350 (94.5 %)	7.79
DSS B		7.270 (92.3 %)	7.370 (93.6 %)	7.87
DSS A	Partial vacuum	7.605 (97.6 %)	7.63 (97.9 %)	7.79
DSS B		7.610 (96.6 %)	7.632 (97.0 %)	7.87

3.1.2. Microstructural analysis

The Fig. 1 shows that the microstructures of solution treated DSS sintered in two dissimilar conditions like hydrogen and partial vacuum. The microstructural photography has clearly indicated that the projection of austenite into ferrite matrix named as Widmanstatten austenitic structure and the equal distribution of duplex phases like dark α ferrite and white (γ) austenite were observed. It was evident that the compositions of DSS in Table 1 which gives the 1:1 ratio of α/γ due to higher Chromium equivalent number of 24.35 (Cr_{eq}) called α stabilizer and higher Nickel equivalent number of 9.12 (Ni_{eq}) called γ stabilizer are important factors that indicates the duplex structures are derived from the equations represented in (1) and (2). The DSS incurred with increased ferrite and austenite of equal proportion due to the complete dissolution of additional alloying elements of Cr, Mo and Ni to the base ferritic and austenitic compositions while the steels are processed at high temperature was known. However, the cooling rate is the key parameter which controls the distribution of alloys. Steels should immediately have cooled by water quench is the significant technique to maintain the precipitate free structure. Chemical analysis of defined grains of 1150 °C solution treated DSS sintered in hydrogen atmosphere and in partial vacuum atmosphere was shown in Table 3 and 4. In recent studies, the presence of fine nano-precipitates in the P91 coarse-grained heat-affected zone (CGHAZ) compared to its P91B counterpart, grain refinement in the fine-grained heat-affected zone (FGHAZ) of both steels with partial dissolution of nano-precipitates, coarsened nano-precipitates in the P91-FGHAZ following post-weld heat treatment, and a mixed structure of partially transformed martensite and coarsened undissolved prior austenite grains with nano-precipitates in the P91 inter-critical heat-affected zone (ICHAZ) as opposed to the P91B-ICHAZ, are the main effects of adding 100 ppm boron to standard P91 steel. These detailed microstructural distinctions further reinforce the significance of alloying elements and heat treatment strategies in tailoring the duplex and heat affected zone microstructures for enhanced performance [31].

By higher the solutionizing temperature, larger the amount of diffusion of alloying elements which increase the grain size of the both regions and it is aided with holding time for 1150 °C held for one hour and sudden quench.

The Fig. 2 shows the SEM images of Solution treated DSSs at different conditions in which the Fig. 2(a) predicts that allotriomorphic ferrite formed as grain boundary contours derived from nucleation at the austenite grain surfaces, and elongated austenite islands. The microstructure of Fig. 1(b) and SEM image of Fig. 2(b) at higher magnification shows that more austenite phases prevail the ferrite due to solution

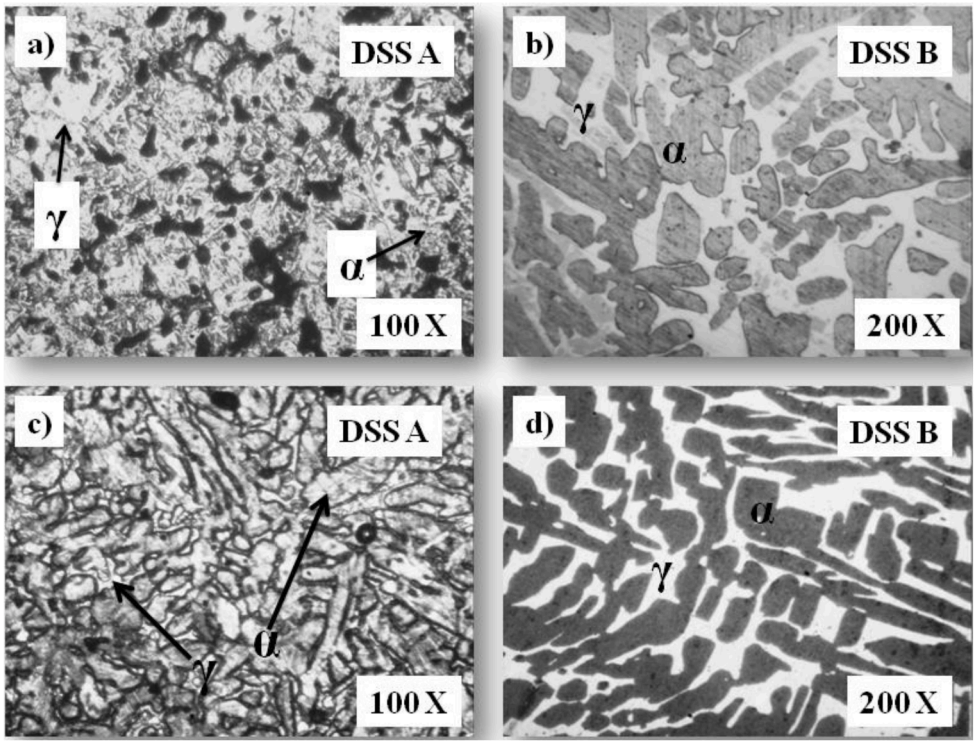

Fig. 1. **(a)** Microstructure of solution treated DSSA at 1150 ℃ sintered in hydrogen (**b)** Microstructure of solution treated DSSB at 1150 ℃sintered in hydrogen **(c)** Microstructure of solution treated DSS A at 1150 sintered℃ in partial vacuum (d) Microstructure of solution treated DSS B at 1150℃ sintered in partial vacuum.

Table 3
Chemical analysis of defined grains of 1150 °C solution treated DSS sintered in hydrogen atmosphere.

Composition	Phase	Elemental concentration wt %					
		Cr	Ni	Mo	Si	Cu	Fe
DSS A	Ferrite	18.42	4.38	0.79	0.86	—	75.56
	Austenite	16.31	6.21	0.67	0.62	—	76.19
DSS B	Ferrite	21.71	5.23	3.80	0.77	—	68.49
	Austenite	17.93	8.59	2.67	0.68	—	70.13

Table 4
Chemical analysis of defined grains of 1150 °C solution treated DSS sintered in partial vacuum atmosphere.

Composition	Phase	Elemental concentration wt %					
		Cr	Ni	Mo	Si	Cu	Fe
DSS A	Ferrite	18.15	7.90	3.49	0.98	—	69.48
	Austenite	17.14	9.72	2.35	0.41	—	70.38
DSS B	Ferrite	20.18	3.45		0.84	—	75.53
	Austenite	15.51	7.27		0.63	—	76.59

annealing temperature and water quench. It was arrived from the microstructural and SEM photography that the solution annealing temperature at 1150 °C aided with optimized soaking time shows the clean austenite and ferrite phase regions and interfaces of ferrite and austenite grains with free of precipitations.

Fig. 3 indicates the SEM–EDS analysis of the α/α (ferrite–ferrite) interface region of DSS B sintered in a hydrogen atmosphere at 1150 °C. As is common for duplex stainless steels treated with high temperatures, the SEM micrograph shows precipitate development localized at the α/α grain boundaries. Silicon (Si), Nickel (Ni), Manganese (Mn) and Molybdenum (Mo) are minor signals in the matching EDS spectrum, which also displays the ferritic matrix's major peaks of iron (Fe) and chromium (Cr). The possible existence of chromium-rich secondary phases, including sigma phase or chromium nitrides, which are frequently linked to solution treatment at intermediate temperatures, is suggested by the notable Cr enrichment at the interface areas. Phase partitioning behaviour during solution treatment is further supported by the interface's comparatively reduced nickel concentration as compared to the matrix. Ultimately, the findings support the idea that ferritic phase stability is enhanced by hydrogen sintering and solution treatment. However, this process also causes localised precipitation at grain boundaries, which, if left unchecked, may affect mechanical and corrosion characteristics.

Following solution treatment at 1150 °C and sintering in a partial vacuum environment, the SEM–EDS analysis of the ferrite zone in DSS B was shown in Fig. 4. The ferritic phase's dominance of iron (Fe) and chromium (Cr), together with trace levels of Ni, Mo, Si, and Mn is confirmed by the EDS spectra. Although there is little nitrogen pickup and austenite regeneration, the microstructure shows a refined and stabilised ferritic phase with less segregation, indicating that partial vacuum sintering in conjunction with high-temperature solution treatment successfully promotes ferrite stabilization.

The ferrite and austenite phases of DSS A and B, solution-treated at 1150 °C and sintered in a hydrogen environment, are chemically analyzed and indicated in Table 3. In comparison to DSS A, DSS B ferrite phase has a noticeably increased molybdenum (Mo) concentration, indicating improved corrosion resistance. In each grade, silicon (Si) showed a very consistent distribution throughout all phases, suggesting no significant propensity towards partitioning. Iron (Fe) was the predominant element in both phases; however, because of the increased alloying element loading overall, its concentration was somewhat lower in DSS B.

The chemical analysis of the ferrite and austenite phases in DSS A and B after solution treatment at 1150 °C and partial vacuum sintering was summarized in Table 4. According to standard elemental partitioning behaviour in duplex stainless steels, DSS A's ferrite phase had a slightly higher concentration of chromium (Cr), while the austenite phase had a larger concentration of nickel (Ni). The ferrite phase has a

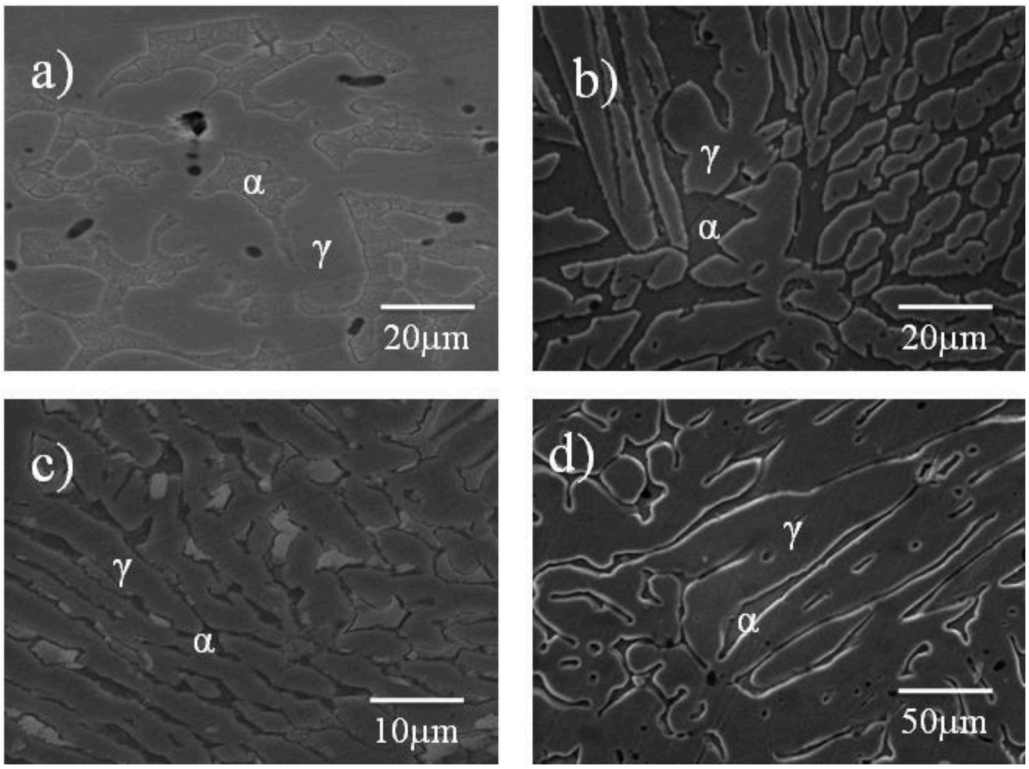

Fig. 2. **(a)** SEM micrographs of DSS A solution treated at 1150°C sintered in hydrogen **(b)** SEM micrographs of DSS B solution treated at 1150°C sintered in hydrogen **(c)** SEM micrograph of solution treated DSS A at 1150°C sintered in partial vacuum **(d)** SEM micrograph of solution treated DSS B at 1150°C sintered in partial vacuum.

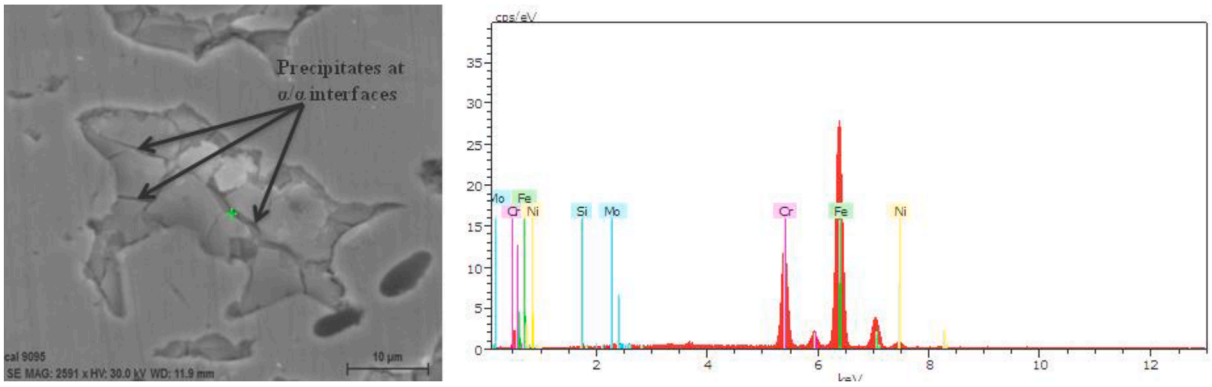

Fig. 3. SEM – EDS of 1150 °C solution treated DSS B (α/α interface region) of sintered in hydrogen atmosphere.

somewhat greater silicon (Si) concentration than the austenite phase. Mo was not found in substantial proportions in either phase, which affected the material's resistance to pitting corrosion. In DSS B, Ni preferred the austenite phase whereas Cr was more concentrated in the ferrite phase. Despite being the predominant element in all phases, iron (Fe) had somewhat reduced concentrations in austenite as a result of enrichment by other alloying elements. Overall, under partial vacuum sintering circumstances, DSS A should provide better corrosion resistance and phase stability than DSS B because to its greater Ni and Mo concentrations.

3.1.3. Ferrite content and mechanical properties

The ferrite content readings of duplex stainless steels (DSS) A and B after solution treatment at 1150 °C in various sintering atmospheres was shown in Table 5. DSS A showed a ferrite content of 22–26 % in the as-sintered state for specimens sintered in a hydrogen environment, which marginally increased to 26–30 % following solution treatment. DSS B, on the other hand, has a substantially greater ferrite concentration, ranging from 40 to 44 % as-sintered to 42–46 % following solution treatment. A similar pattern was seen when sintered in a partial vacuum atmosphere: DSS A showed a ferrite content of 26–28 % as-sintered, rising to 28–32 % after solution treatment, but DSS B retained higher ferrite levels, ranging from 42 to 44 % to 44–48 %. According to these findings, DSS B naturally has a higher ferrite percentage than DSS A. Increased mechanical strength and better resistance to stress corrosion cracking may result from DSS B's greater ferrite content.

The Solution annealed DSS A and B shows higher yield strength than the sintered one in Fig. 2(a) which is apparently indicated by the solution annealing treatment that has accelerated the ferrite contents. Particularly the DSS B shows slight increase in yield strength of 436 MPa than DSS 1 due to density improvement on partial vacuum condition. The DSS A prohibits the elongation was limited to 10 % due to improved

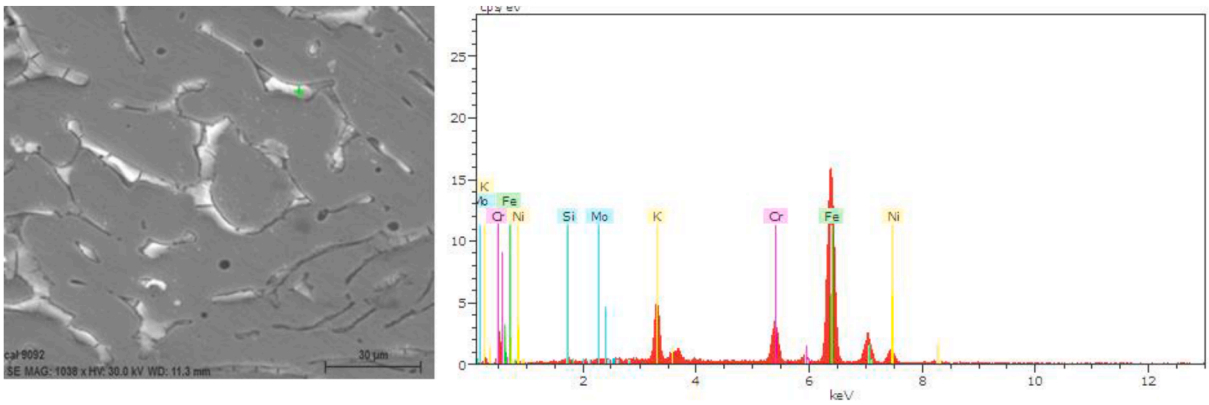

Fig. 4. SEM – EDS of 1150 °C solution treated DSS B (ferrite region) of sintered in partial vacuum atmosphere.

Table 5
Ferrite content measurement of solution treated (1150 °C) DSS.

Composition	Sintered atmosphere	Sintered condition (%)	Solution Treated Condition (%)
DSS A	Hydrogen	22 - 26	26 - 30
DSS B		40 - 44	42- 46
DSS A	Partial Vacuum	26 - 28	28 - 32
DSS B		42 - 44	44 - 48

ferrite content observed in microstructure.

Comparatively the DSS B shows higher tensile strength of 624 MPa and slightly increased elongation is objectionable due to the increased austenite content observed from both the microstructure and SEM analysis in the Fig. 1(b) and Fig. 2(b) and moreover the Fig. 2(c) predicted that reduction on tensile strength after solution annealing. It is obverted to higher amounts of ferrite content of high temperature solution annealing [3,4].Obviously the DSS A has predicted that slight increase in hardness of 70 HRA than the DSS B in Fig. 2(d). Moreover, it is increased due to increased ferrite.

The mechanical characteristics of DSS A and B following solution treatment at 1150 °C in various sintering atmospheres was indicated in Table 6. DSS A demonstrated a 12 % elongation, a tensile strength of 728 MPa, a yield strength of 395 MPa, and a hardness of 65 HRB in hydrogen-sintered conditions. DSS B had a slightly lower tensile strength of 574 MPa and a 10 % decrease in elongation, although having a greater yield strength of 420 MPa and a hardness of 70 HRB. Both materials showed increases in strength qualities when sintered under partial vacuum. With DSS A constantly reaching better tensile strength values and DSS B maintaining greater yield strength and hardness, these results imply that partial vacuum sintering produces superior tensile qualities in both DSS grades as compared to hydrogen sintering.

Table 6
Mechanical properties of solution treated duplex steels at 1150 °C.

Composition	Sintered Atmosphere	Yield Strength (MPa)	Tensile Strength (MPa)	% Elongation	Hardness (HRA)
DSS A	Hydrogen	395	728	12	65
DSS B		420	574	10	70
DSS A	Partial	428	812	12	68
DSS B	vacuum	436	624	12	68

3.2. Solution treated properties at 1250 °C of powder metallurgy DSS sintered in two different atmosphere

3.2.1. Densification characteristics

The densification characteristics of duplex stainless steels (DSS) A and B following solution treatment at 1250 °C in various sintering atmospheres are shown in Table 7. DSS A showed a sintered density of 7.285 g/cm^3 (93.5 % of the theoretical density) for samples sintered in a hydrogen environment. After solution treatment, this density rose to 7.45 g/cm^3 (95.6 %). After treatment, DSS B's sintered density improved to 7.338 g/cm^3 (94.7 %), from a slightly lower 7.270 g/cm^3 (92.3 %). Significantly more densification was attained when partial vacuum sintering was used.DSS B showed an improvement from 7.610 g/cm^3 (96.6 %) to 7.720 g/cm^3 (98.1 %), whereas DSS A achieved a sintered density of 7.605 g/cm^3 (97.6 %), which further increased to 7.654 g/cm^3 (98.3 %) following solution treatment. According to these results, densification was significantly improved by partial vacuum sintering in conjunction with a higher solution treatment temperature of 1250 °C, which brings the materials quite near to their theoretical densities. It was found that improved densification enhanced the treated duplex stainless steels' mechanical strength.

The densities of several DSS under solution-treated and sintered conditions are shown in Fig. 5. It is clear that all DSS variations exhibit a significant increase in density as a result of solution treatment at higher temperatures. The decrease in residual porosity and the encouragement of microstructural homogenization during the solution treatment procedure are responsible for this increase in density. After solution treatment, DSS B exhibits the greatest density among the investigated samples, demonstrating improved phase stability and sintering behaviour. According to these findings, post-sintering thermal treatments are essential for maximizing the densification and general performance of duplex stainless steels.

3.2.2. Microstructural analysis

The duplex structure of the microstructures seen in Fig. 1(a) and (b)

Table 7
Densification properties of solution treated DSS at 1250 °C.

Composition	Sintered atmosphere	Sintered Density (g/cc)	Solution Treated Density (g/cc)	Theoretical Density (g/cc)
DSS A	Hydrogen	7.285 (93.5 %)	7.45 (95.6 %)	7.79
DSS B		7.270 (92.3 %)	7.338 (94.7 %)	7.87
DSS A	Partial vacuum	7.605 (97.6 %)	7.654 (98.3 %)	7.79
DSS B		7.610 (96.6 %)	7.72 (98.1 %)	7.87

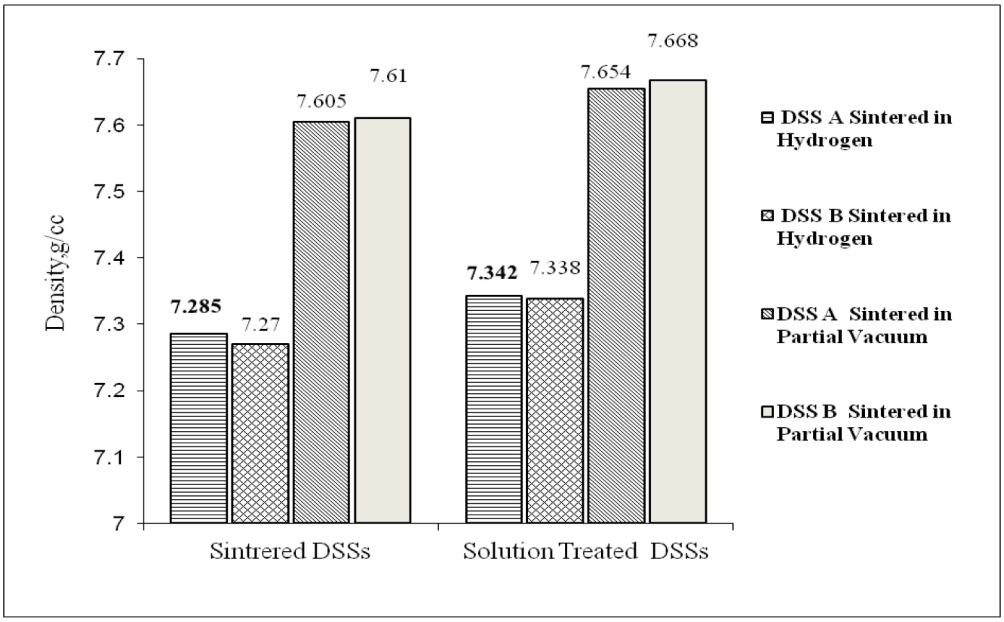

Fig. 5. Densities of different duplex stainless steels both sintered & Solution treated conditions.

is encircled by a dark/grey ferrite matrix and contains austenitic grain, which looks light in colour. Widmanstatten austenite is the name given to the microstructure, which consists of massive ferrite grains with allotriomorphic austenite at the grain borders.

The optical micrographs of DSS solution treated at 1250 °C in various sintering atmospheres are shown in Fig. 6. Effective phase balancing and microstructural refinement owing to solution treatment are demonstrated by the fine and uniform distribution of austenite (γ) islands within a ferritic (α) matrix in DSS A sintered in a hydrogen environment was shown in Fig. 6(a). The significantly coarser microstructure of DSS B sintered in hydrogen in Fig. 6(b), on the other hand, indicates moderate grain development during high-temperature exposure due to its bigger ferrite grains and more isolated austenite areas. Elongated ferrite grains and a smaller volume proportion of austenite

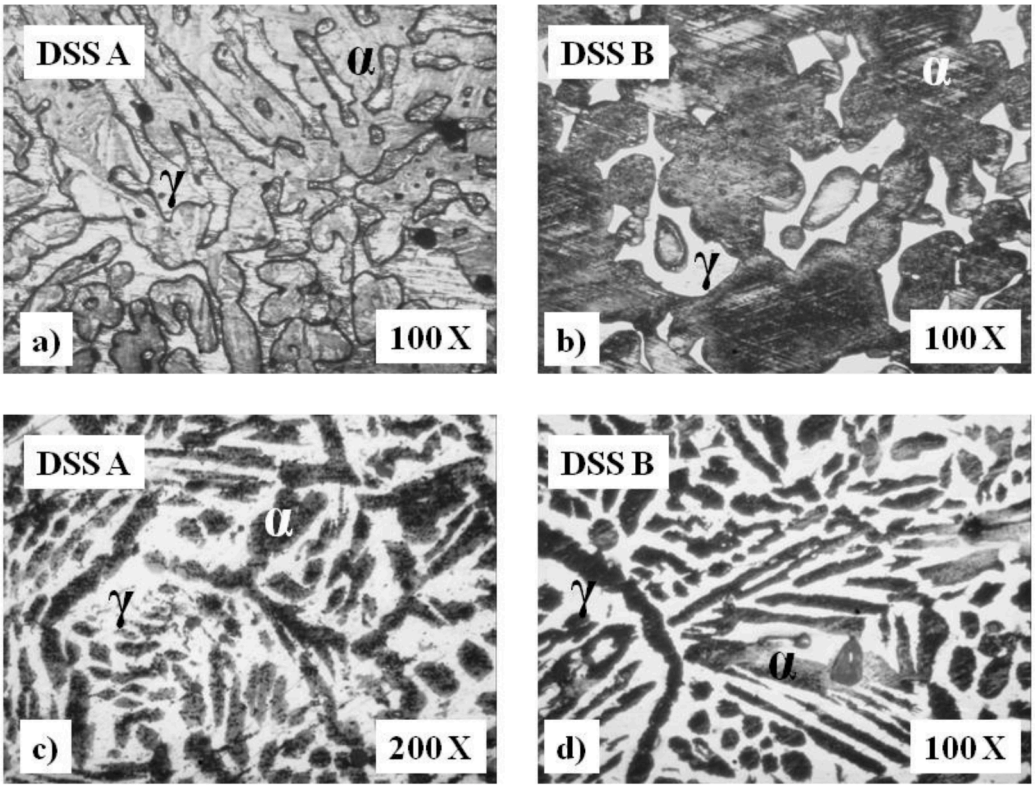

Fig. 6. Optical micrographs of duplex stainless steels Solution treated at 1250 °C **(a)** solution treated DSS A sintered in hydrogen atmosphere **(b)** solution treated DSS B sintered in hydrogen atmosphere **(c)** solution treated DSS A sintered in partial vacuum atmosphere **(d)** Solution treated DSS B sintered in partial vacuum atmosphere.

are seen in DSS A sintered in a partial vacuum environment shown in Fig. 6(c), suggesting directional coarsening and decreased austenite stability due to nitrogen depletion during sintering. Finally, the ferrite-dominated microstructure of DSS B sintered in partial vacuum indicated in Fig. 6(d) is distinguished by prominent ferrite laths and a markedly reduced austenite phase. These findings unequivocally demonstrate how important the sintering atmosphere is in determining the final microstructural morphology, with partial vacuum conditions favouring ferrite grain growth and hindering austenite reformation even after solution treatment, while hydrogen encourages a finer and more balanced duplex structure.

Fig. 7 displays SEM micrographs of DSS solution treated at 1250 °C, highlighting the influence of sintering atmosphere and composition on microstructural evolution. DSS Effective phase restoration following solution treatment is indicated by a fine, balanced duplex structure with distinct austenite islands contained in a ferritic matrix that is sintered in hydrogen in Fig. 7(a). The coarser morphology of DSS B sintered in hydrogen, with well-separated, irregular austenite areas inside ferrite, indicates high phase contrast but modest grain development in Fig. 7(b). DSS despite having significantly longer ferrite grains, a partially vacuum-sintered sample retains a lamellar-like ferrite-austenite configuration, suggesting some directed grain coarsening in Fig. 7(c). Due to reduced nitrogen pickup and changed kinetics in the partial vacuum environment, DSS B sintered in partial vacuum shows a noticeably directed and elongated ferrite structure with sparsely scattered austenite. This suggests ferrite dominance and inhibited austenite regeneration in Fig. 7(d). While partial vacuum sintering tends to favour ferrite coarsening and prevent austenite reformation, the pictures generally demonstrate that hydrogen sintering produces a more refined and balanced duplex microstructure after solution treatment. The refined and balanced duplex structure is primarily accountable for the enhanced tensile characteristics that are shown following solution treatment. Higher ferrite content results in enhanced yield strength and hardness, whereas finely dispersed austenite within the ferrite matrix improves ductility and toughness, demonstrating the microstructure-mechanical connection. Additionally, the mechanical integrity is enhanced by the densification brought about by partial vacuum sintering, which reinforces the grain boundaries and lowers porosity. In line with the microstructure's improved hardness and phase stability, samples with a greater volume % of ferrite showed somewhat less elongation but higher yield strength. Higher yield strength and hardness are a result of the increased ferrite content, whereas ductility and toughness are improved by finely and evenly dispersed austenite islands within the ferrite matrix. Strength is increased by partial vacuum sintering since it reduces porosity and increases phase stability.

A specified austenite grain of solution-treated DSS B sintered in a hydrogen environment is subjected to SEM–EDS analysis, as seen in Fig. 8. As expected from phase partitioning behaviour in duplex stainless steels, the EDS spectrum shows a higher concentration of Ni and a lower proportion of Cr than ferritic areas. Effective stabilisation of the austenite phase is indicated by the existence of notable Fe concentrations as well as small peaks for Mo and Si. The solution treatment at 1250 °C in a reducing hydrogen atmosphere encourages chemical uniformity and improved phase distribution, while the high nickel content helps to stabilise the face-centered cubic (FCC) structure of austenite.

The SEM–EDS analysis of a specific ferrite grain of solution-treated DSS B sintered in a partial vacuum environment is shown in Fig. 9. Iron (Fe) and chromium (Cr), which are indicative of the ferrite phase, are confirmed to be enriched by the EDS spectra. Nickel (Ni), silicon (Si), and molybdenum (Mo) are also found in trace levels; as anticipated, nickel is found in lower proportions than in the austenite phase. Effective phase separation and chemical stabilization during solution treatment are indicated by the high Cr and Fe concentration in the ferrite matrix. A ferrite-dominated microstructure with improved mechanical stability is supported by this composition.

Following solution treatment at 1250 °C and sintering in a hydrogen environment, the chemical analysis of the ferrite and austenite phases of DSS A and B was shown in Table 8. According to standard elemental partitioning in duplex stainless steels, DSS A's ferrite phase had a greater concentration of chromium (Cr) (17.69 wt %) than the austenite phase (15.53 wt %), while the austenite phase had a higher concentration of nickel (Ni) (7.07 wt %) than the ferrite (5.38 wt %). Both phases included silicon (Si) and molybdenum (Mo), with the ferrite having somewhat greater quantities of both elements.With Ni richer in

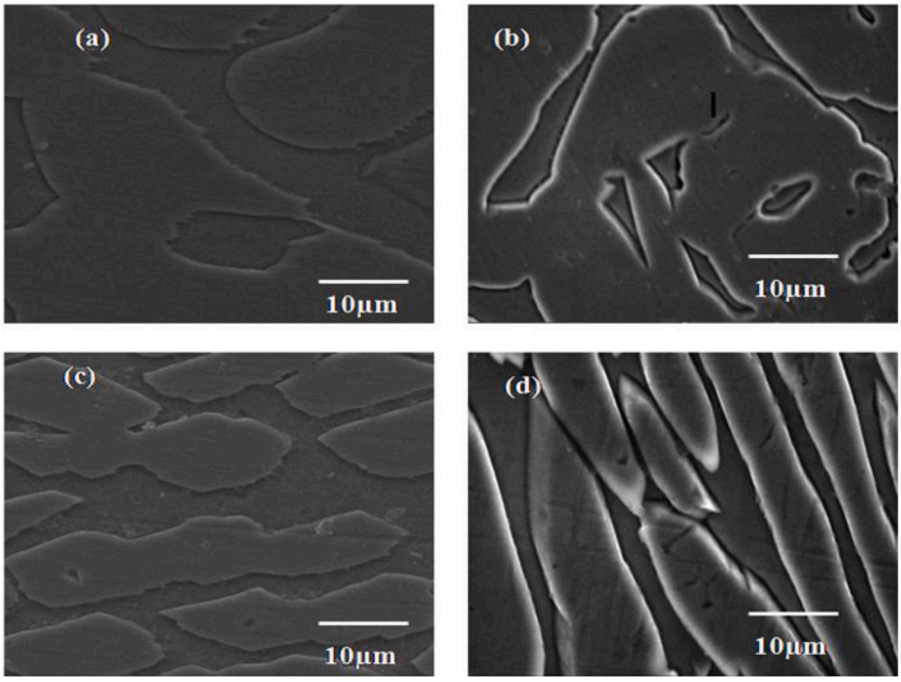

Fig. 7. SEM micrographs of duplex stainless steels Solution treated at 1250 °C **(a)** solution treated DSS A sintered in hydrogen atmosphere **(b)** solution treated DSS B sintered in hydrogen atmosphere **(c)** solution treated DSS A sintered in partial vacuum atmosphere **(d)** solution treated DSS B sintered in partial vacuum atmosphere.

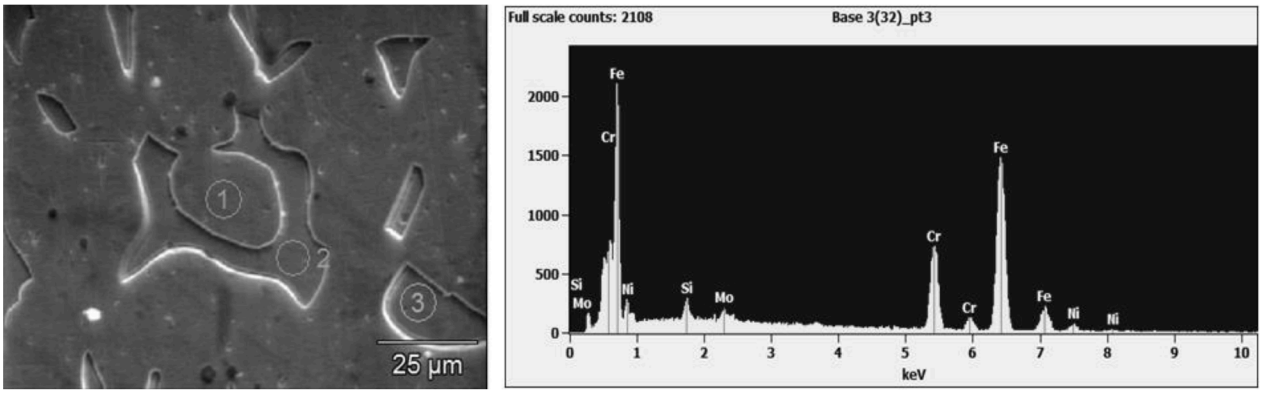

Fig. 8. SEM - EDS analysis on the defined grain (austenite) of solution treated DSS B sintered in hydrogen.

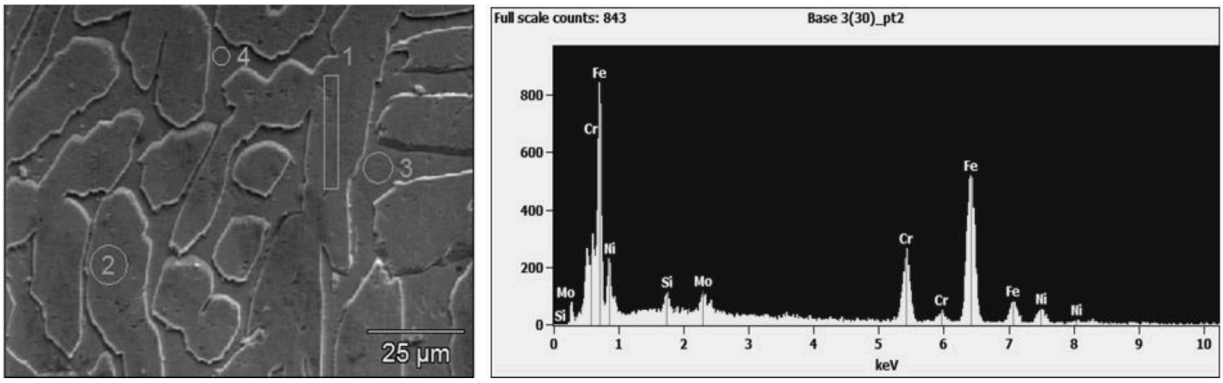

Fig. 9. SEM - EDS analysis on the defined grain (Ferrite) of solution treated DSS B sintered in partial vacuum.

Table 8
Chemical analysis of defined grains of solution treated DSS at 1250 °C sintered in hydrogen atmosphere.

Composition	Elemental concentration wt %						
	Phase	Cr	Ni	Mo	Si	Cu	Fe
DSS A	Ferrite	17.69	5.38	1.00	0.96	—-	74.97
	Austenite	15.53	7.07	0.48	0.74	—-	76.18
DSS B	Ferrite	19.97	3.33	2.21	1.57	—-	72.92
	Austenite	17.43	8.66	0.89	1.09	—-	71.93

Table 9
Chemical analysis of defined grains of solution treated DSS at 1250 °C sintered in partial vacuum atmosphere.

Composition	Elemental concentration wt %						
	Phase	Cr	Ni	Mo	Si	Cu	Fe
DSS A	Ferrite	20.36	7.06	4.60	0.97	—-	67.01
	Austenite	16.64	10.15	2.58	0.86	—-	69.76
DSS B	Ferrite	20.62	10.04	8.59	1.93	—-	58.82
	Austenite	18.76	17.04	3.91	0.37	—-	59.91

austenite (8.66 wt %) and Cr concentration greater in ferrite (19.97 wt %), DSS B showed a similar partitioning tendency. Interestingly, DSS B has more Mo and Si than DSS A, especially in the ferrite phase, which would improve its mechanical strength. All phases showed iron (Fe) as the predominant element, with only slight differences that reflected the relative enrichment of alloying elements. Overall, the findings suggested that elements partitioning between ferrite and austenite is maintained even at higher solution treatment temperatures, and DSS B exhibits a more alloyed composition and provided better performance characteristics.

The chemical analysis of the austenite and ferrite phases in duplex stainless steels (DSS) A and B after partial vacuum sintering and solution treatment at 1250 °C was shown in Table 9. In DSS A, the austenite phase had a substantially greater concentration of nickel (Ni) (10.15 wt %) than the ferrite phase (7.06 wt %), whereas the ferrite phase had a higher concentration of chromium (Cr) (20.36 wt %) than the austenite phase (16.64 wt %). The ferrite phase has much greater molybdenum (Mo) concentrations (4.60 wt %) than the austenite phase (2.58 wt %). Even more alloying was shown in DSS B, where the austenite phase had significant Ni (17.04 wt %), moderate Cr (18.76 wt %), and Mo (3.91 wt %) contents, while the ferrite phase had 20.62 wt % Cr, 10.04 wt % Ni, and 8.59 wt % Mo. In both steels, silicon (Si) was comparatively more abundant in ferrite than in austenite; in the ferrite phase, DSS B had especially high Si. As a result of the increased presence of alloying elements, particularly in DSS B, the iron (Fe) concentration fell accordingly. Overall, the increased quantities of alloying elements, especially in DSS B, indicates improved mechanical strength, with partial vacuum sintering fostering better chemical homogeneity across phases.

The chemical analysis shows that, in comparison to hydrogen sintering, sintering in a partial vacuum environment at 1250 °C produces larger quantities of alloying elements, especially for Mo and Ni. When sintered in partial vacuum, DSS B in particular exhibits a notable increase in Mo content (8.59 wt %) in the ferrite phase, which improved its resistance to corrosion. Furthermore, with partial vacuum sintering, the ferrite phase in both DSS A and B shows a greater Cr and Mo content, suggesting a more alloyed and possibly more durable structure than under hydrogen sintering.

3.2.3. Ferrite content and mechanical properties

The ferrite content readings of DSS A and B following solution

treatment at 1250 °C are displayed in Table 10. DSS A showed a ferrite concentration of 22–26 % in the hydrogen-sintered state, which rose to 34–38 % following solution treatment. After treatment, DSS B's ferrite concentration increased from 40 to 44 % as-sintered to 48–52 %. The ferrite content of DSS A samples that were partially vacuum-sintered increased from 26 to 28 % to 36–38 %, whereas the ferrite content of DSS B samples increased from 42 to 44 % to 50–52 %. With DSS B constantly retaining a greater ferrite percentage, it was found that solution treatment at 1250 °C considerably enhanced the ferrite content in both cases. Additionally, the scientific reason for the increase in ferrite content after solution treatment is that elevated temperatures promote the dissolution of austenite and intermetallic phases into the ferrite phase. This is facilitated by enhanced diffusion kinetics at higher temperatures, leading to a more stabilized ferritic structure and increased ferrite fraction in the microstructure.

The mechanical characteristics of solution-treated DSS at 1250 °C are presented in Table 11. DSS A demonstrated 410 MPa yield strength, 734 MPa tensile strength, and 72 HRA hardness in hydrogen-sintered conditions, whereas DSS B demonstrated 424 MPa, 582 MPa, and 74 HRA, respectively. DSS A maintained a hardness of 72 HRA while achieving an improvement in yield strength to 438 MPa and tensile strength to 824 MPa with partial vacuum sintering. The hardness of DSS B remained at 74 HRA, while its yield strength increased to 444 MPa and its tensile strength to 630 MPa.

Table 10
Ferrite content measurement of solution treated (1250 °C) DSS.

Composition	Sintered atmosphere	Sintered condition (%)	Solution Treated Condition (%)
DSS A	hydrogen	22 - 26	34- 38
DSS B		40 - 44	48- 52
DSS A	partial vacuum	26 - 28	36 – 38
DSS B		42 - 44	50 - 52

Table 11
Mechanical properties of solution treated DSS at 1250 °C.

Composition	Sintered atmosphere	Yield Strength (MPa)	Tensile Strength (MPa)	% Elongation	Hardness (HRA)
DSS A	hydrogen	410	734	10	72
DSS B		424	582	10	74
DSS A	Partial	438	824	10	72
DSS B	vacuum	444	630	10	74

4. Conclusion

The current study significantly assessed how the microstructure and mechanical characteristics of powder metallurgy DSS made from 316 L and 430 L powders were altered by solution treatment temperatures (1150 °C and 1250 °C) and sintering atmospheres (hydrogen and partial vacuum). The following deductions were made:

- The alloying content and heat cycles have a significant impact on microstructure and mechanical response. These results emphasize how crucial processing decisions are to maximizing structural performance.
- Significant improvement in densification was seen following solution treatment at both temperatures. DSS B sintered in partial vacuum had the highest densification, reaching 7.72 g/cm^3 at 1250 °C, or 98.1 % of the theoretical density.
- According to micro-structural study, partial vacuum sintering produced ferrite-rich, elongated morphologies, particularly at higher temperatures, whereas hydrogen sintering encouraged a more balanced duplex structure with a fine and uniform distribution of austenite (γ) and ferrite (α).
- With solution treatment, there was a noticeable change in phase balance. Following solution annealing at 1250 °C, the ferrite content rose from 22 to 26 % to 34–38 % for DSS A and from 40 to 44 % to 48–52 % for DSS B, demonstrating phase change fuelled by heat exposure and quick quenching.
- After solution treatment, especially at 1250 °C, mechanical characteristics were greatly improved. While DSS B demonstrated better hardness (74 HRA), moderate tensile strength (630 MPa), and outstanding ductility (10 % elongation), DSS A, which was sintered in partial vacuum, had the highest tensile strength (824 MPa) and yield strength (438 MPa).
- SEM–EDS analysis verified elemental partitioning, which revealed that austenite phases had greater Ni concentrations while ferrite portions were richer in Cr and Mo. Superior corrosion resistance was suggested by the remarkable Cr (20.62wt %), Ni (10.04wt %), and Mo (8.59wt %) enrichment in ferrite that DSS B sintered in partial vacuum showed.
- Higher Mo and Ni contents, fine phase balance, and reduced secondary phase precipitations—especially following solution treatment at 1250 °C—should result in better corrosion resistance in DSS B.

In overall, the combination of partial vacuum sintering and high-temperature solution treatment was very successful in improving mechanical performance, microstructural uniformity, and densification. For demanding applications like oil and gas pipelines, chemical processing industries, marine environments, and high-performance structural components that demand an exceptional blend of strength, ductility and optimized DSS materials created by this process are promising options.

Ethics approval

Not applicable.

Consent to participate and publication

Not applicable.

CRediT authorship contribution statement

Ramajayam Mariappan: Writing – original draft, Investigation. **Rasaiah Naveenkumar:** Writing – review & editing, Conceptualization. **Thangaraj Vinod Kumar:** Visualization, Validation, Supervision. **Vadivelu Kannan:** Writing – review & editing, Supervision, Conceptualization. **Prajith Prabhakar:** Visualization, Validation, Conceptualization. **Vinayagam Mohanavel:** Visualization, Validation. **Manickam Ravichandran:** Visualization, Validation, Supervision, Conceptualization.

Declaration of competing interest

The authors declare that they have no known competing financial interests or personal relationships that could have appeared to influence the work reported in this article.

Data availability

No data was used for the research described in the article.

References

[1] S.L. Dos Santos, S.F. Santos, Heat treatment of the SAE 9254 spring steel: influence of cooling rate on the microstructure and microhardness, Next Mater. 3 (2024) 100175, https://doi.org/10.1016/j.nxmate.2024.100175.

[2] E. Akshaya Devi, C. Ravi, Stability of B1-type oxides in BCC iron studied using density functional theory calculations, Mater. Today Commun. 25 (2020) 101266, https://doi.org/10.1016/j.mtcomm.2020.101266.
[3] H. Tan, Y. Jiang, B. Deng, T. Sun, J. Xu, J. Li, Effect of annealing temperature on the pitting corrosion resistance of super duplex stainless steel UNS S32750, Mater. Charact. 60 (2009) 1049–1054, https://doi.org/10.1016/j.matchar.2009.04.009.
[4] R.A. Perren, T. Suter, C. Solenthaler, G. Gullo, P.J. Uggowitzer, H. Bohni, M. O. Speidel, Corrosion resistance of super duplex stainless steels in chloride ion containing environments: investigations by means of a new microelectrochemical method. II. influence of precipitates, Corros. Sci. 43 (2001) 727–745, https://doi.org/10.1016/S0010-938X(00)00088-3.
[5] J. Wang, Y. Kang, H. Yu, W. Ge, Effect of quenching temperature on microstructure and mechanical properties of Q1030 steel, Mater. Sci. Appl 10 (2019) 665–675, https://doi.org/10.4236/msa.2019.1010047.
[6] K.P. Davidson, R. Liu, C. Zhu, M. Cagiciri, L.P. Tan, A. Alagesan, S. Singamneni, Effect of build orientation and heat treatment on the microstructure, mechanical and corrosion performance of super duplex stainless steels fabricated via laser powder bed fusion, Mater. Adv. 5 (2024) 8177–8198, https://doi.org/10.1039/d4ma00448e.
[7] J. Kunz, A. Boontanom, S. Herzog, P. Suwanpinij, A. Kaletsch, C. Broeckmann, Influence of hot isostatic pressing post-treatment on the microstructure and mechanical behavior of standard and super duplex stainless steel produced by laser powder bed fusion, Mater. Sci. Eng. A. 794 (2020) 139806, https://doi.org/10.1016/j.msea.2020.139806.
[8] G.N. Nigon, O. Burkan Isgor, S. Pasebani, The effect of annealing on the selective laser melting of 2205 duplex stainless steel: microstructure, grain orientation, and manufacturing challenges, Opt. Laser Technol. 134 (2020) 106643, https://doi.org/10.1016/j.optlastec.2020.106643.
[9] F. Hengsbach, P. Koppa, K. Duschik, M.J. Holzweissig, M. Burns, J. Nellesen, W. Tillmann, T. Troster, K.P. Hoyer, M. Schaper, Duplex stainless steel fabricated by selective laser melting - microstructural and mechanical properties, Mater. Des. 133 (2017) 136–142, https://doi.org/10.1016/j.matdes.2017.07.046.
[10] P. Manikandan, K. Venkatesan, Role of volumetric energy density on surface quality and mechanical properties of selective laser melted 310 stainless steel, Results Eng. 25 (2025) 104479, https://doi.org/10.1016/j.rineng.2025.104479.
[11] P. Murkute, S. Pasebani, O.B. Isgor, Effects of heat treatment and applied stresses on the corrosion performance of additively manufactured super duplex stainless steel clads, Materialia 14 (2020) 100878, https://doi.org/10.1016/j.mtla.2020.100878.
[12] X. Zhao, A. Wang, J. Wang, C. Ling, X. Gui, Study on the effect of solid solution treatment on the microstructure evolution and properties of 304 stainless steel bellows, Results Eng. 26 (2025) 104565, https://doi.org/10.1016/j.rineng.2025.104565.
[13] A.S. Siahaan, S. Ishihara, Y. Sasaki, H. Kawai, T. Nagasaka, Thermo-viscoelastic mechanical behavior and fractography analysis of lean duplex stainless steel SUS821L1, Results Eng. 27 (2025) 105911, doi: 10.1016/j.rineng.2025.105911.
[14] Y. Zhang, F. Cheng, S. Wu, Improvement of pitting corrosion resistance of wire arc additive manufactured duplex stainless steel through post-manufacturing heat-treatment, Mater. Charact. 171 (2021) 110743, https://doi.org/10.1016/j.matchar.2020.110743.
[15] S.K. Ghosh, S. Mondal, High temperature ageing behaviour of a duplex stainless steel, Mater. Charact. 59 (2008) 1776–1783, https://doi.org/10.1016/j.matchar.2008.04.008.
[16] Z. Que, P.A. Ferreiros, J. Li, Y. Wang, L. Chang, W. Gong, X. Wang, Corrosion behavior in lead-bismuth eutectic of 316 L stainless steels fabricated by laser-based powder bed fusion and powder metallurgy-hot isostatic pressing, Corros. Sci. 251 (2025) 112911, https://doi.org/10.1016/j.corsci.2025.112911.
[17] H. Tian, X. Cheng, Y. Wang, C. Dong, X. Li, Effect of Mo on interaction between α/γ phases of duplex stainless steel, Electrochim. Acta 267 (2018) 255–268, https://doi.org/10.1016/j.electacta.2018.02.082.
[18] R. Bao, E.B. Farfán, B. Li, C. Bao, Preparation and erosion resistance properties of 00Cr22Ni6MnMoCu duplex stainless steel, Results Eng. 26 (2025) 105004, doi: 10.1016/j.rineng.2025.105004.
[19] N.D. Fahad, N.S. Radhi, Z.S. Al-Khafaji, A.A. Diwan, Surface modification of hybrid composite multilayers spin cold spraying for biomedical duplex stainless steel, Heliyon 9 (2023) e14103, https://doi.org/10.1016/j.heliyon.2023.e14103.
[20] A.B. Tahchieva, N. Llorca-Isern, J.M. Cabrera, Duplex and superduplex stainless steels: microstructure and property evolution by surface modification processes, Metals 9 (2019) 347, https://doi.org/10.3390/met9030347.
[21] R. Kumar, K. Kishore, N. Shajan, D. Vijay Kumar, B. Nirmal Kumar K, A. Prabhakaran, S.K. Paul, M. Tiwari, K.S. Arora, Surface & Coatings Technology effect of number of deposition layers on the microstructure, corrosion and fretting wear of duplex stainless-steel weld cladding, Surf. Coat. Technol. 502 (2024) 131924, https://doi.org/10.1016/j.surfcoat.2025.131924.
[22] L. Becker, J. Boes, J. Lentz, C. Cui, M. Steinbacher, Y.L. M, R. Fechte-heinen, W. Theisen, S. Weber, Influence of annealing time on the microstructure and properties of additively manufactured X2CrNiMoN25 –7 –4 duplex stainless steel: experiment and simulation, Materialia 28 (2023) 101720, https://doi.org/10.1016/j.mtla.2023.101720.
[23] X. Zhu, L. Dong, G. Li, X. Li, Materials science & engineering a laser powder bed fusion of 2507 duplex stainless steel: microstructure, mechanical properties, and corrosion performance, Mater. Sci. Eng. A. 913 (2024) 147084, https://doi.org/10.1016/j.msea.2024.147084.
[24] M. Akhtar, A. Khajuria, Probing true microstructure-hardening relationship in simulated heat affected zone of P91B steels, Metallogr. Microstruct. Anal. 8 (2019) 656–677, https://doi.org/10.1007/s13632-019-00573-w.
[25] A. Singh, A. Khajuria, R. Bedi, S.G. Dommeti, S. Shiva, Microstructural and mechanical property analysis of high-strength low-alloy steel tubes fabricated using wire arc-directed energy deposition technique, Met. Mater. Int. 31 (2025) 1815–1835, https://doi.org/10.1007/s12540-024-01849-9.
[26] A. Khajuria, S. Shiva, A. Misra, Comparative study of fillers for welding E410 structural steel, Adv. Mater. Process. Technol. (2024) 1–21, https://doi.org/10.1080/2374068X.2024.237969.
[27] A. Khajuria, A. Misra, S. Shiva, On the heat-affected zone role for mechanical properties of structural-steel MIG and CMT–MIG weldments, Trans. Indian. Inst. Met. 77 (2024) 3905–3913, https://doi.org/10.1007/s12666-024-03460-3.
[28] S. Sengottaiyan, V.S. Shaisundaram, M. Shameer Basha, B. Deepanraj, N. Senthilkumar, Effect of duplex and austenite stainless steel fillers on mechanical, microstructural, and corrosion characteristics of dissimilar welds using cold metal transfer welding, Results Eng. 26 (2025) 104818, https://doi.org/10.1016/j.rineng.2025.104818.
[29] A. Khajuria, M. Akhtar, R. Bedi, R. Kumar, M.K. Ghosh, C.R. Das, S.K. Albert, Influence of boron on microstructure and mechanical properties of Gleeble simulated heat-affected zone in P91 steel, Int. J. Press. Vessels Pip. 188 (2020) 104246, https://doi.org/10.1016/j.ijpvp.2020.104246.
[30] A. de A. Vicente, P.A. D'Silva, I.L. Dos Santos, R.R. de Aguiar, A.B. Botelho Junior, T.F. de A. Santos, The effect of shielding gases in the ferrite number of austenitic stainless steels joints through GMAW, Int. J. Adv. Eng. Res. Sci. 7 (2020) 332–341, https://doi.org/10.22161/ijaers.77.37.
[31] A. Khajuria, M. Akhtar, R. Bedi, Boron addition to AISI A213/P91 steel: preliminary investigation on microstructural evolution and microhardness at simulated heat-affected zone, Future Mater. Sci. Eng. Technol. 53 (2022) 1167–1183, https://doi.org/10.1002/mawe.202100152.